Radio Science, Volume 16, Number 6, pages 1183–1199, November–December 1981

Modeling attenuation and phase of radio waves in air at frequencies below 1000 GHz

Hans J. Liebe

National Telecommunications and Information Administration, Institute for Telecommunication Sciences
Boulder, Colorado 80303

(Received December 10, 1980; revised January 25, 1981; accepted February 27, 1981.)

Moist air is characterized for the frequency range 1–1000 GHz as a nonturbulent propagation medium described by meteorological parameters. An adequate spectroscopic data base for air consists of three terms: (1) resonance information for 29 H_2O lines up to 1097 GHz and 44 O_2 lines up to 834 GHz in the form of intensity coefficients and center frequency for each line; (2) an empirical water vapor continuum spectrum; and (3) a liquid water attenuation term for haze and cloud conditions. This data base is the heart of two computer programs which calculate and plot attenuation rates (in decibels per kilometer), refractivity (in parts per million), and refractive dispersion (in parts per million). The first covers the troposphere and requires pressure, temperature, and relative humidity as input data. The second addresses isolated line behavior in the mesosphere wherein the geomagnetic field strength H is an additional input parameter due to the Zeeman effect of the O_2 molecules. Each oxygen line splits proportionally with H into numerous sublines, which are juxtaposed to form Zeeman patterns spread over a megahertz scale. Patterns of three main polarization cases are considered. Various typical examples for a model atmosphere demonstrate the utility of the approach, provide new information, and underline the serious role that water vapor plays above 120 GHz.

1. INTRODUCTION

The physical properties of the neutral atmosphere influence radio wave propagation. For the frequency range 1–1000 GHz, inherent losses are due to spectral absorption by the molecules H_2O and O_2. Further propagation limitations are caused by turbulence and atmospheric layering effects, and by thermal noise emitted from the absorbing air mass. Intermittently, of course, rain is the dominant absorber, at least in the 15- to 500-GHz range [*Crane*, 1981].

With the current high interest in millimeter and submillimeter waves, there is need for a reliable model to predict average loss and delay effects from easy-to-obtain meteorological data. Such a model would find considerable practical application through conversion of basic climatological variables (i.e., barometric pressure P, temperature T, relative humidity RH) into transfer characteristics of a radio path. The frequency of 1000 GHz is a kind of new frontier for a growing technology encompassing microwave and optical principles. Millimeter wave systems are attractive because of their ability to penetrate a somewhat opaque atmosphere (haze, fog, clouds, dust, smoke, light rain) under circumstances in which electro-optical and infrared systems normally fail. Accurate and detailed knowledge of atmospheric transmission properties is essential in evaluating the advantages that millimeter waves might have over shorter wavelengths.

Water in both vapor and liquid states is the major deterrent to an unrestricted exploitation of millimeter and, more so, of infrared wavelengths. For most applications, the operation of ground-based systems is limited in frequency to window regions $W1$–$W5$, these being the gaps between molecular absorption lines and bands as schematically given in Table 1.

Mean values and limits of the following propagation effects: absorptive loss of coherent radiation, time of propagation between two points (both of which are discussed in this paper), refractive ray bending, generation of incoherent noise, and scintillations due to random fluctuations of the medium in space and time, can be considered for modeling. The characteristics of a short, horizontal radio path are approximately modeled by one value of an average complex refractivity N. Cumulative behavior (e.g., a ground-to-satellite path) is calculated by assuming a spherically stratified atmosphere in which each layer has a constant N value. This

Paper number 1S0352.

TABLE 1. Millimeter wave window ranges of the atmosphere.

Absorption feature	Window range (GHz)	Attenuation range at sea level (dB/km)
22-GHz H_2O line		
*W*1	24–48	0.1–0.3
60-GHz O_2 line complex		
*W*2	70–110	0.3–1
119-GHz O_2 line		
*W*3	120–155	1–2.5
183-GHz H_2O line		
*W*4	190–300	2–10
325-GHz H_2O line		
*W*5	335–355	5–20
380-GHz H_2O line (and 1823 more lines of the rotational band up to 25 THz)		

layer-by-layer method uses numerical integration techniques. Refinements consider refractive and dispersive ray bending at low elevation angles [*Hopponen*, 1980].

Since the pioneering work by *Van Vleck* [1947] and *Birnbaum* [1953] much progress has been made in describing atmospheric millimeter wave spectra. Recent advances are in the spectroscopic data base [*Liebe et al.*, 1977; *Poynter and Pickett*, 1980; *Rothman*, 1981], in line shape theory [*Rosenkranz*, 1975; *Lam*, 1977; *Smith and Guiraud*, 1979; *Smith*, 1981], in measurements of refraction [*Kemp et al.*, 1978], in modeling [*Falcone et al.*, 1979; *Hopponen*, 1980; *Hill and Clifford*, 1981], in reporting anomalous window absorption [*Emery et al.*, 1980], in collecting available field data to support an empirical water vapor continuum [*Crane*, 1980], in reviewing window excess absorption [*Liebe*, 1980], in treating liquid water uptake in clear-to-hazy air at high relative humidities [*Nilsson*, 1979], and in the submillimeter wave dielectric constant for water [*Simpson et al.*, 1979]. A unified model of these new results is given in two computer programs: Program P1 covers attenuation rates $\alpha(f)$ and dispersion $D(f)$ in the height range h = 0–30 km; Program P2 calculates isolated line behavior especially Zeeman patterns of oxygen lines in the mesophere (h = 30–100 km). Both programs are formulated in engineering terms and are fully traceable, but void of quantum-mechanical complications. They can serve as a reference for comparisons with future data, which are presently very scarce for the 200- to 1000-GHz range. In this range, the computation rests foremost on theory, while the confidence limit below 100 GHz is estimated to be better than 4%, based on extensive laboratory testing.

In the past, computer programs were written [*Falcone et al.*, 1979; *Harries*, 1980; *Hill et al.*, 1980] with spectral line data drawn from the Air Force Geophysics Laboratory tape (*Rothman* [1981] and *Rothman et al.* [1981]; these compilations are available as the main atlas of some 159,000 transitions and a minor constituents atlas in the form of magnetic tapes from the National Climatic Center of the National Oceanic and Atmospheric Administration, Digital Product Section, Federal Building, Asheville, North Carolina). The sheer number of lines ($>10^5$) makes such calculations quite time-consuming, nontransparent, and costly. Up to 1000 GHz, the two principal absorbing species are H_2O and O_2, and simplifications can be employed such as (1) an intensity cutoff ($>2 \times 10^{-3}$ dB/km at line center) to reduce the number of contributing lines and (2) an adjustable resolution factor determining the frequency grid for plotting, which still captures all extremes without an excessive number of steps. On the other hand, important additions are the overlap correction for the 60-GHz O_2 band and the Zeeman splitting matrices for mesospheric O_2 lines.

2. REFRACTIVITY OF MOIST AIR

Amplitude and phase response of a planar radio wave traveling the distance L and starting with the field strength E_0 is described by

$$E = E_0 \exp(\Gamma L) = E_0 \exp[j0.02096f(10^6 + N)L] \quad (1)$$

Frequency f is in gigahertz (GHz) throughout the paper and Γ is the propagation constant.

Germane to any propagation model is a convenient macroscopic measure of the interaction between radiation and the absorbing species in moist air. Complex refractivity N (in parts per million), expressed in terms of measurable quantities, provides that role. For air, N consists of three components

$$N = N_0 + D(f) + jN''(f) \quad \text{ppm} \quad (2)$$

namely, the frequency independent refractivity N_0 plus various spectra of refractive dispersion $D(f)$ and absorption $N''(f)$. Usually, the imaginary part of (2) is expressed as the specific power attenuation

α and the real part determines the phase delay β (with reference to vacuum); that is,

$$\alpha = 0.1820 f N'' \quad \text{dB/km}$$
$$\beta = 0.02096 f (N_0 + D) \quad \text{radians/km} \tag{3a}$$

Accordingly, the propagation constant Γ and the excess propagation delay time t are

$$\Gamma = -0.1151\alpha + j(2.096 \times 10^4 f + \beta) \quad 1/\text{km}$$
$$t = (\beta/2\pi f)10^3 = 3.336(N_0 + D) \quad \text{ps/km} \tag{3b}$$

An overview of notation used to formulate $\alpha(N'')$ and $\beta(N_0, D)$ is given in Table 2.

The physical state of moist air, which determines the absorber population in a radio path, is described by

- p dry air pressure (barometric pressure $P = p + e$), kPa (1 kPa = 10 mbar);
- ϑ relative inverse temperature, equal to $300/T$ (T in °K);
- e water vapor partial pressure, kPa;
- w liquid water concentration, g/m^3.

The number M of O_2^{16} (20.845% in dry air) and H_2O molecules per unit air volume is given by the ideal gas law:

$$M(O_2 + H_2O) = (0.5034p + 2.415e)\vartheta\, 10^{17} \quad \text{cm}^{-3} \tag{4}$$

Thus p-e-ϑ combinations account for the number of molecular absorbers in moist air. In the water vapor state, the saturation pressure e_s at a given 'temperature' ϑ_1 (dew point) cannot be exceeded; that is [*Bögel*, 1977],

$$e \le e_s = 2.409\vartheta_1^5 \times 10^{(10-9.834\vartheta_1)} \quad \text{kPa} \tag{5}$$
$$e_s \approx 3.5\vartheta^{18}$$

(Equation (5) describes the data of the standard Smithsonian Meteorological Tables to within ±0.2% for the range ±40°C.) The vapor pressure with respect to saturation defines relative humidity as

$$RH \equiv (e/e_s)100 \leqq 100\% \tag{6}$$

The humidity condition $RH = 100\%$ is a delicate balance point for physical phase changes. A drop of 1 K decreases the water vapor in saturated air between 5% (40°C) and 8% (−10°C). The excess water vapor pressure $e_x = e(\vartheta_1) - e_s(\vartheta_1^* > \vartheta_1)$ is converted into a liquid water droplet concentration

$$w = 7.219 e_x \vartheta_1^* \quad \text{g/m}^3 \tag{7}$$

The conversion process, however, starts well below

TABLE 2. Notation overview.

	Notation	Unit of measurement
Propagation parameters		
Frequency	f (1)	GHz
Attenuations	α (3), α_w (22), α_l (25), $\alpha_{1,3}$ (28), α_z (29)	dB/km
Refractivities, dispersion	N (1), N_0 (10), N'' (11), N_c'' (20), (21), D (12)	ppm
Orientation angle	θ (29)	
Attenuation response	δ (Figure 9)	%
Physical measurables		
Height	h (9)	km
Pressure, temperature, relative humidity	$P(h)$, $T(h)$, $RH(h)$ (9)	kPa, K, %
Magnetic field strength	H (26)	G
Physical variables		
Molecular number density, relative mass	M (4), m (23)	cm^{-3}, 1
Relative temperature, dew point	ϑ (4), ϑ_1 (5)	1
Partial pressures	p, e (4), e	kPa
Droplet concentration	w (7)	g/m^3
Spectroscopic parameters		
Line shapes, strength	F'' (13), F' (14), S (17)	GHz^{-1}, MHz
Center frequency, widths, overlap	ν_0 (13), γ (17), γ_D (23), ∂ (17)	GHz, GHz, 1
Line coefficients	$a_{1,-5}$, $b_{1,-1}$ (17)	(see Table 4)
Zeeman shift and relative strength	η (26), ξ (27)	1
Transition labels	π, $\sigma^{\pm}$ (Table 6)	
O_2 quantum numbers	K, M (Table 6)	
Complex dielectric constant of water	$\epsilon = \epsilon' + j\epsilon''$ (22a)	1

Number in parentheses denotes equation where symbol is defined.

TABLE 3. The model atmosphere (U.S. Standard Atmosphere, 1976).

Height, h (km)	Dry air pressure, p	Temperature, T (°K)	Maximum relative humidity $(RH)_0$ (%)	Magnetic field strength H (G)	Program	Temperature parameter, $\vartheta = 300/T$	Saturation pressure, e, (equation (5)) (Pa)
0	101.325 kPa	288.15	100		P1	1.041	1706
1.6	83.527 kPa	277.75	100			1.080	847.7
3	70.121 kPa	268.66	100			1.117	434.0
6	47.217 kPa	249.19	100*		1–1000 GHz	1.204	88.1
10	26.499 kPa	223.25	60			1.344	6.41
16	10.352 kPa	216.65	3			1.385	(1.72)†
20	5.529 kPa	216.65	2			1.385	(1.72)†
30	1.197 kPa	226.51	1			1.324	9.36
30	1197.000 Pa	226.51		0.2–0.8	P2	1.324	
40	287.140 Pa	250.35		0.2–0.8		1.198	
50	79.779 Pa	270.65		0.2–0.8		1.108	
60	21.958 Pa	247.02		0.2–0.8		1.215	
70	5.221 Pa	219.59		0.2–0.8	$\nu_0(O_2)$	1.366	
80	1.052 Pa	198.64		0.2–0.8	±50 MHz	1.510	
90	0.184 Pa	187.21		0.2–0.8		1.603	
100	0.032 Pa	198.99		0.2–0.8		1.508	

*Height profiles of humidity above h = 6 km are discussed by *Ellsaesser et al.* [1980].
†Value over ice.

RH = 100% due to water uptake by suspended, invisible aerosol particles [*Nilsson*, 1979]. The liquid water concentration in 'clear' air with RH > 70% can range somewhere between

$$w(RH) = 0.001 \quad \text{and} \quad 0.1 \ \text{g/m}^3 \tag{8}$$

The objective at this point is to express the quantities $\alpha(f)$, $D(f)$, and N_0 in terms of p-e-ϑ-w data, subject to the following conditions:

Frequency

$$f = 1\text{–}1000 \ \text{GHz}$$

Altitude

$$h = 0\text{–}100 \ \text{km} \tag{9}$$

Relative humidity

$$RH = 0\text{–}100\%$$

Magnetic field strength

$$H = 0.1\text{–}0.8 \ \text{gauss (G)}$$

Numerical and graphical examples are then calculated for the model atmosphere specified in Table 3, using various combinations of (9).

The frequency-independent refractivity is given by [*Liebe et al.*, 1977]

$$N_0 = 2.589p\vartheta + 41.6e\vartheta^2 + 2.39e\vartheta \quad \text{ppm} \tag{10}$$

and can be calculated in a straightforward manner. Water vapor refractivity is about 16 times more effective, on a per molecule basis, than dry air in generating propagation phenomena such as delay, ray bending, ducting, scintillations, etc.

The absorption and dispersion spectra are formulated from line contributions, a continuum N''_c, and a liquid water extinction N''_w; i.e.,

$$N''(f) = \sum_i (SF'')_i + N''_c + N''_w \quad \text{ppm} \tag{11}$$

and

$$D(f) = \sum_i (SF')_i \quad \text{ppm} \tag{12}$$

Both expressions require more elaboration, as detailed below.

First, the line spectra of absorption SF'' and of refractive dispersion SF' have strength S in units of kilohertz and shape factors F' and F'' in units of $(\text{GHz})^{-1}$. The summations consider i = 44 O_2 plus 29 H_2O lines (line spectra of the trace gases O_3, CO, N_2O, SO_2, NH_3, etc. [*Waters*, 1976; *Poynter and Pickett*, 1980; *Rothman*, 1981; *Rothman et al.*, 1981] are neglected). Common to each line

is a pair of intensity-versus-frequency distribution functions [e.g., *Waters*, 1976; *Kemp et al.*, 1978]. In the atmosphere, the shape factors named after Van Vleck-Weisskopf (VVW) and Gross are used. We chose the VVW shape as modified by *Rosenkranz* [1975]:

$$F'' = \left(\frac{f}{\nu_0}\right)\left[\frac{\gamma - (\nu_0 - f)\partial}{(\nu_0 - f)^2 + \gamma^2} + \frac{\gamma - (\nu_0 + f)\partial}{(\nu_0 + f)^2 + \gamma^2}\right] \quad (13)$$

and

$$F' = \left[\frac{(\nu_0 - f) + \gamma\partial}{(\nu_0 - f)^2 + \gamma^2} + \frac{(\nu_0 + f) + \gamma\partial}{(\nu_0 + f)^2 + \gamma^2} - \frac{2}{\nu_0}\right] \quad (14)$$

where ν_0 is the molecular line center frequency, γ is the width, and $\partial < \pm 1$ is the overlap interference. Above heights of about 15 km, isolated line behavior takes over, limiting each molecular resonance to a megahertz scale frequency span. For isolated line calculations, (13) and (14) can be replaced by Lorentzian shapes

$$F''_i = \gamma / [(\nu_0 - f)^2 + \gamma^2]$$
$$F'_i = (\nu_0 - f) / [(\nu_0 - f)^2 + \gamma^2] \quad (15)$$

Maximum absorption at $f = \nu_0$ and peak dispersion at $f = \nu_0 \mp \gamma$ are given by

$$N''_m = S/\gamma \qquad \pm D_m = S/2\gamma \quad \text{ppm} \quad (16)$$

The line parameters are calculated as follows [*Liebe and Gimmestad*, 1978]:

	O_2 in air
S, kHz	$a_1 p \vartheta^3 \exp[a_2(1-\vartheta)]$
γ, GHz	$a_3(p + 1.3e)\vartheta^{0.9}$
∂	$a_4 p \vartheta^{a_5}$

(17)

	H_2O in air
S, kHz	$b_1 e \vartheta^{3.5} \exp[b_2(1-\vartheta)]$
γ, GHz	$b_3(4.80e + p)\vartheta^{0.6}$
∂	0

An invariable line-data base (ν_0 and the spectroscopic coefficients $a_{1\text{-}5}$, $b_{1\text{-}3}$) is used in conjunction with meteorological conditions expressed through sets of p-ϑ-e data. The line base is derived from experiments [*Liebe et al.*, 1977; *Kemp et al.*, 1978] and spectroscopic parameter compilations [*Poynter and Pickett*, 1980; *Rothman*, 1981] and is listed in Table 4. Line intensities (equation (16)) of a few selected lines are independent of temperature when

	$T = 273$ $\vartheta = 1.1$	150 K 2.0
$a_2 = 2.1 \ln \vartheta/(\vartheta - 1)$	2.00	1.46
$b_2 = 2.9 \ln \vartheta/(\vartheta - 1)$	2.76	2.02

(18)

Lines with a_2, b_2 coefficients lower than those prescribed by (18) increase in intensity when the temperature drops and vice versa.

Dispersion $D(f)$ addresses only frequency dependent contributions. The term $2/\nu_0$ is the finite value of the first two terms in the shape factor $F'(f)$ when $f \to 0$ and, consequently, is subtracted from (14). Without this measure, for example, the sum of all rotational H_2O lines (that is, 1838 lines between 22 GHz and 31 THz) is close (−2.5%) to the measured dipole orientation term $41.6e\vartheta^2$ in (10) [*Hill and Clifford*, 1981], while the lines listed in Table 4 yield a residual contribution fitted by

$$N'_R = \sum_i [SF'(f \to 0)]_i$$
$$\doteq (4.75e + 1.14 \times 10^{-3} p)\vartheta^3 \quad \text{ppm} \quad (19)$$

Second, the continuum spectrum $N''_c = N''_v + N''_d$ consists of N''_v, the far-wing absorption by very strong infrared H_2O lines (plus additional contributions which are not fully understood) and N''_d, the nonresonant dry air spectrum. We opted for the empirical expression [*Waters*, 1976]

$$N''_v \approx 1.9 f e p \vartheta^{3.1} \times 10^{-6} \quad \text{ppm} \quad (20a)$$

which fitted available field data reasonably well [*Crane*, 1980].

The magnitude of N''_v is about a factor of 5 above the far-wing contribution (first term of (20*b*)), which is computed when the complete rotational H_2O spectrum is taken into account. The excess absorption, so far, has not found a generally acceptable explanation. An earlier laboratory experiment by us yielded (for $f < 100$ GHz)

$$N''_{vx} \approx (0.24 f^{1.3} e p \vartheta^{3.5} + 2.2 f^{1.6} e^2 \vartheta^{12}) \times 10^{-6} \quad \text{ppm} \quad (20b)$$

The correct magnitude of N''_v is a major factor in the window ranges *W*2–*W*5. In view of the conflicting evidence [*Liebe*, 1980], the alternatives of either (20*a*) or (20*b*) are not too different (see Figure 2 in section 3). Various researchers have conjectured

TABLE 4a. Data base for O_2 (a_1-a_5) and H_2O (b_1-b_5) spectral lines in air.

Center frequency, ν_0 (GHz)	Strength, a_1 (kHz/kPa)	Temperature exponent, a_2	Width, a_3 (GHz/kPa)	Interference, a_4 (1/kPa)	Temperature exponent, a_5	Quantum number identification, K^2
0[a]	0.307 E−3 (ppm/kPa)		0.12 (0.056) E−1			1[+] to 37[+]
50.47381	0.94 E−6	0.969 E+1	0.86 E−2	0.520 E−2	0.179 E+1	37[−]
50.98742	0.244 E−5	0.869 E+1	0.87 E−2	0.550 E−2	0.169 E+1	35
51.50311	0.604 E−5	0.774 E+1	0.89 E−2	0.560 E−2	0.177 E+1	33
52.02124	0.141 E−4	0.684 E+1	0.92 E−2	0.550 E−2	0.181 E+1	31
52.54227	0.308 E−4	0.600 E+1	0.94 E−2	0.569 E−2	0.179 E+1	29
53.06683	0.637 E−4	0.522 E+1	0.97 E−2	0.528 E−2	0.189 E+1	27
53.59570	0.124 E−3	0.448 E+1	0.100 E−1	0.544 E−2	0.183 E+1	25
54.12997	0.2265 E−3	0.381 E+1	0.102 E−1	0.480 E−2	0.199 E+1	23
54.67115	0.3893 E−3	0.319 E+1	0.105 E−1	0.484 E−2	0.190 E+1	21
55.22137	0.6274 E−3	0.262 E+1	0.1079 E−1	0.417 E−2	0.207 E+1	19
55.78382	0.9471 E−3	0.212 E+1	0.1110 E−1	0.375 E−2	0.207 E+1	17
56.26477	0.5453 E−3	0.100 E−1	0.1646 E−1	0.774 E−2	0.890	D1[b] 1[+]
56.36339	0.1335 E−2	0.166 E+1	0.1144 E−1	0.297 E−2	0.229 E+1	15[−]
56.96818	0.1752 E−2	0.126 E+1	0.1181 E−1	0.212 E−2	0.253 E+1	13[−]
57.61249	0.2125 E−2	0.910	0.1221 E−1	0.940 E−3	0.376 E+1	11[−]
58.32389	0.2369 E−2	0.621	0.1266 E−1	−0.550 E−3	−0.111 E+2	D2 9
58.44658	0.1447 E−2	0.827 E−1	0.1449 E−1	0.597 E−2	0.790	3[+]
59.16422	0.2387 E−2	0.386	0.1319 E−1	−0.244 E−2	0.700 E−1	7[−]
59.59098	0.2097 E−2	0.207	0.1360 E−1	0.344 E−2	0.490	5[+]
60.30604	0.2109 E−2	0.207	0.1382 E−1	−0.435 E−2[c]	0.680	D3 5[−]
60.43478	0.2444 E−2	0.386	0.1297 E−1	0.132 E−2	−0.120 E+1	7[+]
61.15057	0.2486 E−2	0.621	0.1248 E−1	−0.360 E−3	0.584 E+1	9[+]
61.80016	0.2281 E−2	0.910	0.1207 E−1	−0.159 E−2	0.286 E+1	11[+]
62.41122	0.1919 E−2	0.126 E+1	0.1171 E−1	−0.266 E−2	0.226 E+1	D4 13[+]
62.48626	0.1507 E−2	0.827 E−1	0.1468 E−1	−0.503 E−2[c]	0.850	3[−]
62.99797	0.1492 E−2	0.166 E+1	0.1139 E−1	−0.334 E−2	0.218 E+1	15[+]
63.56852	0.1079 E−2	0.212 E+1	0.1108 E−1	−0.417 E−2	0.196 E+1	17[+]
64.12778	0.7281 E−3	0.262 E+1	0.1078 E−1	−0.448 E−2	0.200 E+1	19[+]
64.67886	0.4601 E−3	0.319 E+1	0.105 E−1	−0.515 E−2	0.184 E+1	21[+]
65.22412	0.2727 E−3	0.381 E+1	0.102 E−1	−0.507 E−2	0.192 E+1	23[+]
65.76474	0.152 E−3	0.448 E+1	0.100 E−1	−0.567 E−2	0.178 E+1	25[+]
66.30195	0.794 E−4	0.522 E+1	0.97 E−2	−0.549 E−2	0.184 E+1	27[+]
66.83663	0.391 E−4	0.600 E+1	0.94 E−2	−0.588 E−2	0.174 E+1	29[+]
67.36933	0.181 E−4	0.684 E+1	0.92 E−2	−0.560 E−2	0.177 E+1	31[+]
67.90051	0.795 E−5	0.774 E+1	0.89 E−2	−0.580 E−2	0.173 E+1	33[+]
68.43054	0.328 E−5	0.869 E+1	0.87 E−2	−0.570 E−2	0.165 E+1	35[+]
68.95972	0.128 E−5	0.969 E+1	0.86 E−2	−0.530 E−2	0.174 E+1	37[+]
118.75034	0.9341 E−3	0.000	0.1592 E−1	−0.441 E−3	0.890	1

that possible sources of the excess absorption are hydrogen-bonded dimers and/or clusters of selective size distributions (10–30 H_2O molecules) [*Carlon and Harden*, 1980]. Clustering is assumed to take place during the evaporation process. Another line of thought holds the *RH*-dependent H_2O attachment to hygroscopic foreign matter (aerosol water uptake) responsible—a kind of 'invisible' cloud [*Nilsson*, 1979].

The nonresonant air spectrum N''_d makes, at sea level pressures, a small contribution. The formulation

$$N''_d = 6.2fp\theta^2 \times 10^{-4}$$

TABLE 4b. Data base for O_2 (a_1–a_5) and H_2O (b_1–b_3) spectral lines in air ($a_4 = a_5 = b_4 = b_5 = 0$).

Center frequency, ν_0 (GHz)	Strength, a_1 (kHz/kPa)	Temperature exponent, a_2	Width, a_3 (GHz/kPa)	Quantum number identification (O_2)	
				Lower	Upper
368.498350	0.679 E−4	0.200 E−1	0.156 E−1	1, 1	2, 3
424.763120	0.638 E−3	0.122 E−1	0.147 E−1	2, 1	2, 3
487.249371	0.235 E−3	0.122 E−1	0.147 E−1	2, 1	3, 3
715.393150	0.996 E−4	0.891 E−1	0.144 E−1	3, 3	4, 5
773.839732	0.571 E−3	0.798 E−1	0.140 E−1	4, 3	4, 5
834.145790	0.180 E−3	0.798 E−1	0.140 E−1	4, 3	5, 5
				Identification (H_2O)	
ν_0	b_1	b_2	b_3	Lower	Upper
• 22.235080	0.105	0.214 E+1	0.281 E−1	5, 2, 3	6, 1, 6
68.052	0.180 E−2	0.875 E+1	0.280 E−1	3, 2, 1 (1)[d]	4, 1, 3
• 183.310091	0.238 E+1	0.653	0.282 E−1	2, 2, 0	3, 1, 3
321.225644	0.460 E−1	0.616 E+1	0.220 E−1	9, 3, 6	10, 2, 9
• 325.152919	0.155 E+1	0.152 E+1	0.290 E−1	4, 2, 2	5, 1, 5
• 380.197372	0.123 E+2	0.102 E+1	0.285 E−1	3, 2, 1	4, 1, 4
386.778	0.400 E−2	0.733 E+1	0.160 E−1	11, 2, 10	10, 3, 7
437.34667	0.630 E−1	0.502 E+1	0.150 E−1	6, 6, 0	7, 5, 3
439.150812	0.921	0.356 E+1	0.175 E−1	5, 5, 0	6, 4, 3
443. 018295	0.191	0.502 E+1	0.148 E−1	6, 6, 1	7, 5, 2
• 448.001075	0.107 E+2	0.137 E+1	0.246 E−1	3, 3, 0	4, 2, 3
470.888947	0.328	0.357 E+1	0.181 E−1	5, 5, 1	6, 4, 2
474.689127	0.124 E+1	0.234 E+1	0.210 E−1	4, 4, 0	5, 3, 3
488.491133	0.256	0.281 E+1	0.222 E−1	7, 1, 7	6, 2, 4
504.219	0.380 E−1	0.669 E+1	0.127 E−1	7, 7, 0	8, 6, 3
505.126	0.120 E−1	0.669 E+1	0.130 E−1	7, 7, 1	8, 6, 2
• 556.936002	0.526 E+3	0.114	0.317 E−1	1, 0, 1	1, 1, 0
• 620.700807	0.521 E+1	0.234 E+1	0.216 E−1	4, 4, 1	5, 3, 2
658.340	0.460	0.776 E+1	0.328 E−1	1, 0, 1 (1)	1, 1, 0
• 752.033227	0.259 E+3	0.336	0.302 E−1	2, 0, 2	2, 1, 1
836.836	0.120 E−1	0.811 E+1	0.170 E−1	11, 2, 9	10, 5, 6
859.810	0.150 E−1	0.799 E+1	0.270 E−1	2, 0, 2 (1)	2, 1, 1
899.380	0.910 E−1	0.784 E+1	0.300 E−1	1, 1, 1 (1)	2, 0, 2
903.280	0.640 E−1	0.835 E+1	0.280 E−1	2, 2, 1 (1)	3, 1, 2
907.773	0.179	0.504 E+1	0.204 E−1	8, 3, 5	9, 2, 8
• 916.169	0.890 E+1	0.137 E+1	0.249 E−1	3, 3, 1	4, 2, 2
970.320	0.940 E+1	0.184 E+1	0.246 E−1	4, 3, 1	5, 2, 4
• 987.940	0.145 E+3	0.180	0.299 E−1	1, 1, 1	2, 0, 2
• 1097.368	0.840 E+3	0.656	0.335 E−1	3, 0, 3	3, 1, 2

Read 0.307 E−3 as 0.307×10^{-3}.

[a] Nonresonant O_2 spectrum (equation (21)).

[b] D1 denotes doublet.

[c] *Rosenkranz*'s [1975] first-order solution for the 60-GHz band shape has a shortcoming: the listed values of $a_4(K = 3^-, 5^-)$ have to be reduced 5% (which is of negligible consequence) to assure that $\alpha(O_2) \geq 0.000$ for $f > 160$ GHz even when $N''_d = 0$ (equation (21).

[d] Here (1) denotes first vibrationally excited state.

$$\{[\gamma_0/(f^2 + \gamma_0^2)] + 2.1p\vartheta^{0.5} \times 10^{-7}\} \quad \text{ppm} \qquad (21)$$

(O_2) (N_2)

is taken from *Rosenkranz* [1975] (nonresonant O_2) and *Stankevich* [1974] (pressure-induced N_2). The width γ_0 is calculated with (17) and $a_3 = 0.012$ GHz/kPa [*Lam*, 1977], albeit the value $a_3 = 0.0056$ generated the a_4 and a_5 coefficients (Table 4) using *Rosenkranz*'s [1975] scheme to fit laboratory data [*Liebe et al.*, 1977]. This discrepancy has been resolved in a more profound theoretical treatment

TABLE 5. Cloud (fog, haze) attenuation α_w in decibels per kilometer for 1 g/m^3 liquid water content at 0° and 25°C.

	Frequency f, GHz									
	1	10	30	100	200	300	400	600	800	1000
				Equation (22a)						
α_w at 0°C	0.001	0.097	0.82	5.4	9.3	10.7				
α_w at 25°C	0.001	0.051	0.45	4.2	10.8	15.3				
				Equation (22b)						
α_w at 0°C							13	18	23	29
α_w at 25°C							21	31	40	48

of the 60-GHz band shape by *Smith* [1981].

Third, the liquid water extinction N''_w of droplets with radii smaller than 20 μm (cloud, haze, aerosol hydrometeors) can be derived from published dielectric data of bulk water (ε', ε''). The Rayleigh absorption approximation

$$N''_w = 4.49 w \varepsilon'' / [(\varepsilon' + 2)^2 + (\varepsilon'')^2] \quad \text{ppm} \qquad (22a)$$

of Mie scattering losses is appropriate up to 1000 GHz [*Falcone et al.*, 1979]. Frequency and temperature dependences of ε', ε'' are calculated with the Debye model given by *Chang and Wilheit* [1979], which was found to describe available experimental data up to 300 GHz.

At frequencies $f \geq 300$ GHz, the rough approximation

$$N''_w \approx 0.55 w f^{0.1} \vartheta^{6} \quad \text{ppm} \qquad (22b)$$

was obtained [*Liebe*, 1980] by fitting ε data reported for the submillimeter wave range [e.g., *Simpson et al.*, 1979]. Some numerical examples of the attenuation $\alpha_w = 0.182 f N''_w$ (in decibels per kilometer) are listed in Table 5. Equations (22*a*) and (22*b*) are applied to model the attenuation by aerosols, haze, clouds, and fog if their average water concentration and temperature within a radio path are known.

3. THE TROPOSPHERE PROGRAM P1

The complex refractivity N (equation (2)), as formulated in the previous section, is applied in a computer routine (P1) to generate values of attenuation $\alpha(f)$, dispersion $D(f)$, and refractivity N_0 (equation (10)). The program is valid for frequencies up to 1000 GHz and for heights up to 30 km. In the troposphere ($h < 10$ km), only lines of H_2O and O_2 are important. Above $h = 10$ km, the weak spectral signatures of trace gases (O_3, CO, N_2O, etc.) become detectable, but are not included in the described model. The calculation of $N(f, P, T, RH)$ is done in a subroutine using line-by-line superposition at each frequency. Relative humidity RH is specified and controls, through (5), the water vapor pressure. A liquid water concentration w can be added. Attenuation α requires (3), (5), (6), (11), (13), (17), (20*a*), (21), and (22); similarly, for refractive dispersion D, (2), (3), (5), (6), (12), (14), and (17) are applied.

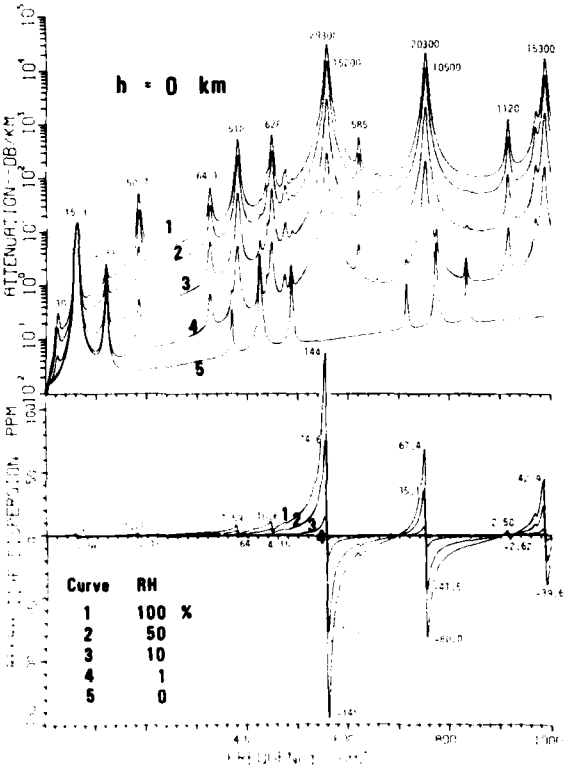

Fig. 1. Attenuation α in decibels per kilometer and refractive dispersion D in parts per million for dry ($RH = 0\%$) to saturated ($RH = 100\%$) air at sea level ($h = 0$ km) (see Table 3) over the frequency range $\nu = 1$–1000 GHz. Some check values are listed below.

	α, dB/km		
f, GHz	$RH = 0$	10	100%
10	0.016	0.017	0.028
50	0.299	0.322	0.527
100	0.054	0.136	0.886
200	0.028	0.546	5.38
300	0.040	0.982	9.71
500	0.108	11.1	116
1000	0.284	124	1313

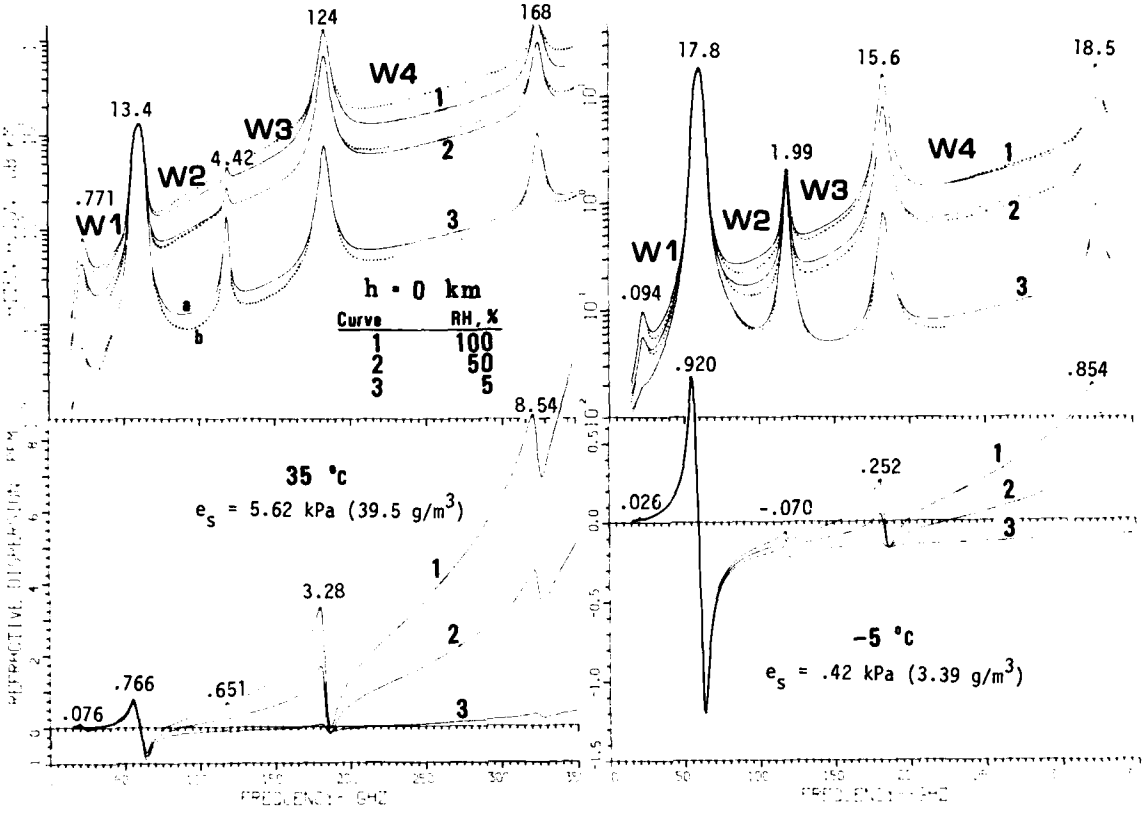

Fig. 2. Attenuation α in decibels per kilometer and refractive dispersion D in parts per million of dry (RH = 5%), humid (RH = 50%), and saturated (RH = 100%) air at sea level (h = 0 km) for temperatures T = −5°C (15°C—see Figure 1) and 35°C over the frequency range ν = 15–350 GHz. Continuum model 'a' uses equation (20*a*) and 'b' uses (20*b*).

The main program P1 generates a frequency grid with a resolution that is tied to the line center frequencies which fall within the desired range. Two consecutive values of ν_0 are taken from Table 4, and the number of points in between them is specified (usually 2–5). Also automatically added to the grid are the half-power points at $\nu_0 \pm \gamma$. Thus it is assured that attenuation maxima and dispersion peaks are not missed. The program feeds one frequency at a time into the subroutine and receives values of α and D, which are stored temporarily in two files. When all numbers of the grid have been processed, the output is presented in a numerical printout and processed by a graphics routine. Examples are depicted in Figures 1–4 taking $w = 0$. Some obvious conclusions drawn from these figures are as follows.

An overview to 1000 GHz at sea level is given in Figure 1. Water vapor attenuation above 125 GHz extends up to 3×10^4 dB/km. The strongest maxima of the rotational H_2O spectrum, however, are two orders of magnitude higher and fall in the 2- to 12-THz range [*Hill et al.*, 1980]. Transmission below 25 THz over any distance is, for practical purposes, limited to the window ranges *W*1–*W*4 below 350 GHz. The low-frequency wing of the dispersion spectrum, originating from the strong 557-GHz H_2O line, makes its influence known down to about 100 GHz.

Atmospheric EHF (30–300 GHz) transfer properties are exemplified in Figure 2 at sea level for the temperatures −5° and +35°C and the difference between the two water vapor continuum spectra (20*a*) and (20*b*) is illustrated. The transparency of

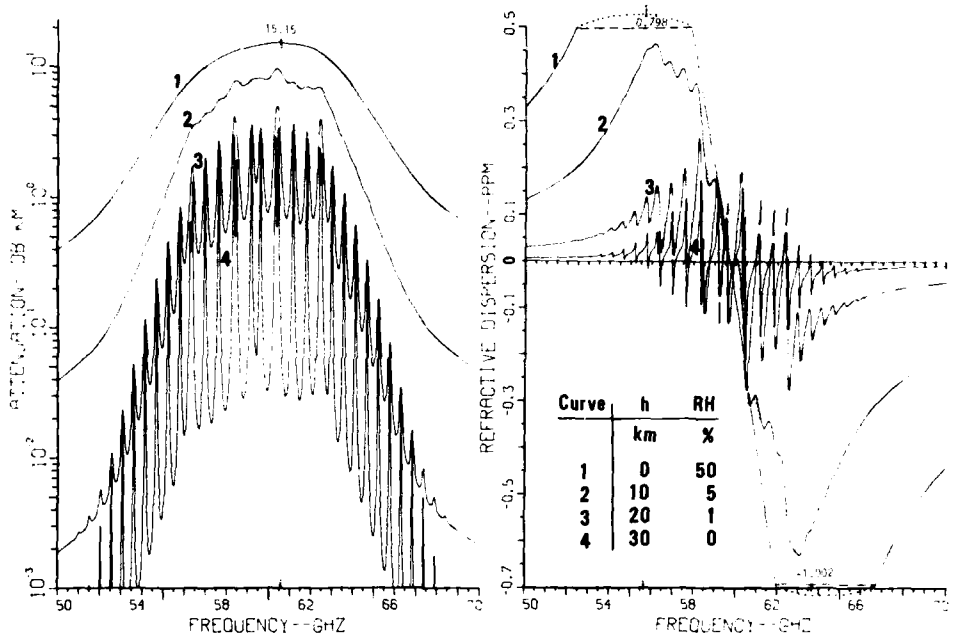

Fig. 3. Attenuation α in decibels per kilometer and refractive dispersion D in parts per million for the oxygen microwave band at the altitudes h = 0–30 km (see Table 3) covering the frequency range ν = 50–70 GHz.

the window ranges *W2–W4* is dominated by the controversial water vapor excess absorption, which is normally modeled by (20*a*). The temperature dependence of window attenuation, expressed in terms of e, is only T^{-1}, but changes to T^{17} when *RH* is the governing variable. A more detailed picture of molecular attenuation appears in Figure 3. The oxygen microwave spectrum dominates in the range 50–70 GHz. Close to sea level the 60-GHz lines are merged into an unstructured band shape, the maximum intensity of which is pressure-proportional until the lines separate ($h > 15$ km). Above 15 km, the overlap disappears and radio channels with up to 400-MHz bandwidth can be accommodated between the lines. Details of the center portion of the 60-GHz band are magnified in Figure 4. This figure shows interesting dispersion properties, which change with increasing height from negative to positive gradients $dD/d\nu$ between the 5$^+$ and 5$^-$ lines. Numerical values depicted in Figures 1, 2, and 4 may serve as control numbers for Program P1.

4. THE MESOSPHERE PROGRAM P2

Program P2 calculates the attenuation of single lines as they appear above h = 30 km. The formulation starts with an isolated, pressure-broadened line described by (3) and (11) for $N''_c = 0$, (15), (16), and (17). Decreasing pressure in (17) eventually approaches the finite Doppler line width

$$\gamma_D = 6.20\nu_0/\sqrt{m\vartheta} \quad \text{kHz} \tag{23}$$

where m is the molecular weight (e.g., O_2, m = 32, ϑ = 1, ν_0 = 60 GHz; γ_D = 65.8 kHz). As a consequence, a change to a Gaussian line shape function takes place.

The convolution of Lorentzian and Gaussian shape functions is called the Voigt profile, which is governed by the parameter $y = \gamma/\gamma_D$ and which is appropriate when this ratio falls in the range ≈10–0.1. Numerical evaluation of the height-dependent, complex Voigt function requires considerable computational effort. Usually, the Voigt profile 'frequencies' x and 'pressures' y are normalized in multiples of γ_D and the intensities are expressed with reference to the Lorentzian shape. Frequency profiles reduced in such a manner are labeled for absorption $u(x, y) = F''/F'_L$ and for dispersion $v(x, y) = F'/F''_L$. Examples are shown in Figure 5 together with the pressure profiles of the two maxima u_0 and v_0 approaching zero intensity. Maxi-

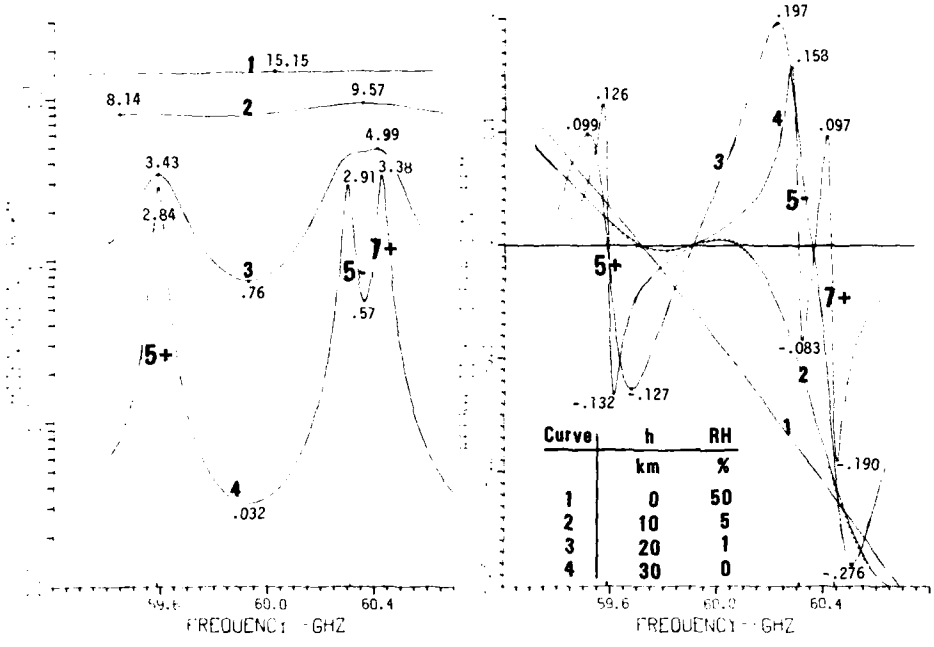

Fig. 4. Attenuation α in decibels per kilometer and refractive dispersion D in parts per million at the oxygen microwave band center for the altitudes h = 0–30 km (see Table 3) covering the frequency range ν = 59.4–60.7 GHz.

mum line attenuation is followed by P2 through the mesophere until it has dropped below 0.01 dB/km. A FORTRAN IV algorithm was adopted for the calculations of $u(x, y)$ as reported by *Pierluissi et al.* [1977]. An adequate approximation can be made by replacing γ in (17) with

$$\gamma_h = \sqrt{\gamma^2 + \gamma_D^2} \tag{24}$$

and keeping the shape functions (equations (15)). Isolated line attenuation is then simply ((3), (11), (15), (16), and (24)) given by

$$\alpha_i(f) = \alpha_0/(1 + z^2) \quad \text{dB/km} \tag{25}$$

where $\alpha_0 = 0.1820fS/\gamma_h$ is the maximum at ν_0, and $z = (\nu_0 - f)/\gamma_h$ is the normalized frequency.

Zeeman splitting of isolated oxygen lines due to the influence of the earth's magnetic field strength H introduces considerable complications [*Lenoir*, 1968]. The presence of the steady field H (in units of gauss) splits each of the K^+ lines into three groups of $(2K^+ \pm 1)$ sublines, thereby redistributing

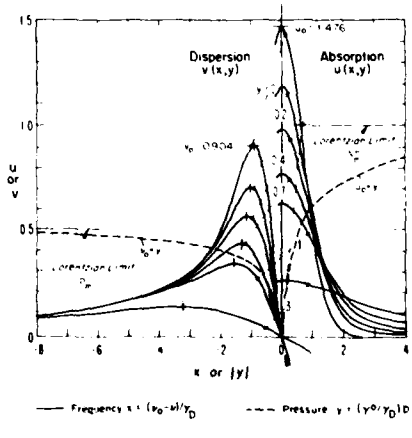

Fig. 5. Normalized Voigt profiles [*Faddeyea and Tarentev*, 1961] for absorption $u(x, y)$ and dispersion $v(x, y)$. Shown are frequency profiles ($\nu = f$) at p = const (solid curves) and pressure profiles of maximum absorption $u_0 y$ and peak dispersion $|v_0 y|$ (dashed curves). For O_2 lines, $\gamma^0 = a_1\vartheta^{0.8}$, and for H_2O lines, $\gamma^0 = b_1\vartheta^{0.6}$.

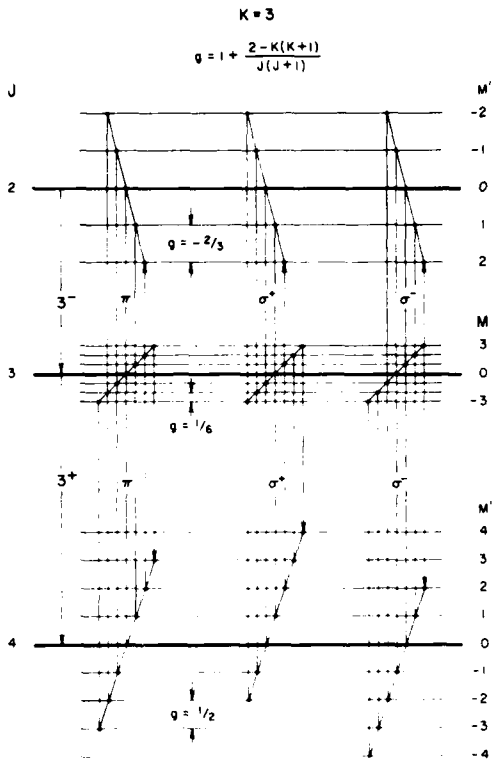

Fig. 6. Schematic energy level diagram displaying the Zeeman components for $K = 3^-$ and 3^+ oxygen microwave lines. K is total rotational angular momentum quantum number in odd integers, $J = K$ and $K \pm 1$ is the rotational quantum number, M is the magnetic quantum number (Table 6), and g is the Landé splitting factor.

the line attenuation α_i (equation (25)) over a fixed frequency range.

Part of program P2 is a subroutine which calculates the line center frequencies

$$\nu_0^- = \nu_0 + \eta(K, M)28.03 \times 10^{-4} H \quad \text{GHz} \tag{26}$$

and the line strength coefficients

$$a_i^- = a_i \xi(K, M) \quad \text{kHz/kPa} \tag{27}$$

for the Zeeman components of each K^- microwave line. The components are identified by the magnetic quantum number M. The rotational quantum number J, which is determined by the total quantum number K, sets the limits on M. Figure 6 gives an example of the schematic distribution of energy levels and allowed transitions for the case $K = 3$. The Landé g factor is the constant of proportionality for a splitting of each J level. The fact that g is different for levels $J > 1$ leads to the anomalous Zeeman effect, while the two lines $K = 1^-$ display the normal Zeeman effect. The calculation procedure for the relative frequency shifts $\eta(K, M)$ and relative intensities $\xi(K, M)$ is summarized in Table 6. The formulations are based on *Lenoir*'s [1968] work with two exceptions: (1) the intensities $\xi(K, M)$ are normalized to the theoretical definition of the coefficient a_1 [*Liebe and Gimmestad*, 1978], and (2) both K lines are referred, against convention for K^+, to the same set of M values (see Figure 6), which leads to the limits of M specified in Table 6. An O_2 line breaks up into numerous components, which are organized in three groups labeled π, σ^+, and σ^-.

TABLE 6. Relative frequency shift $\eta(M, K)$ and relative intensity factor $\xi(M, K)$ for Zeeman components of O_2 microwave lines.

Attenuation rate	Zeeman transitions	K^- line		K^+ line	
		$\eta(M, K) < \pm 1$	$\xi(M, K) < 1$	$\eta(M, K) < \pm 1$	$\xi(M, K) \le 1$
α_1	π	$\frac{M(1-K)}{K(K+1)}$	$\frac{3[(K+1)^2 - M^2]}{(K+1)(2K+1)(2K+3)}$	$\frac{M(K+2)}{K(K+1)}$	$\frac{3(K+1)(K^2 - M^2)}{K(2K+1)(2K^2+K-1)}$
	$(\Delta M = 0)$	M limits: $\pm M \le K$		$K - 1 \ge M \ge -(K-1)$	
α_2	σ^-	$\frac{M(1-K) - K}{K(K+1)}$	$\frac{3(K+M+1)(K+M+2)}{4(K+1)(2K+1)(2K+3)}$	$\frac{(M+1)(K+2) - 1}{K(K+1)}$	$\frac{3(K+1)(K-M)(K-M-1)}{4K(2K+1)(2K^2+K-1)}$
	$(\Delta M = 1)$	M limits: $\pm M \le K$		$K - 2 \ge M \ge -K$	
α_3	σ^+	$\frac{M(1-K) + K}{K(K+1)}$	$\frac{3(K-M+1)(K-M+2)}{4(K+1)(2K+1)(2K+3)}$	$\frac{(M-1)(K+2) + 1}{K(K+1)}$	$\frac{3(K+1)(K+M)(K+M-1)}{4K(2K+1)(2K^2+K-1)}$
	$(\Delta M = -1)$	M limits: $\pm M \le K$		$K \ge M \ge -(K-2)$	

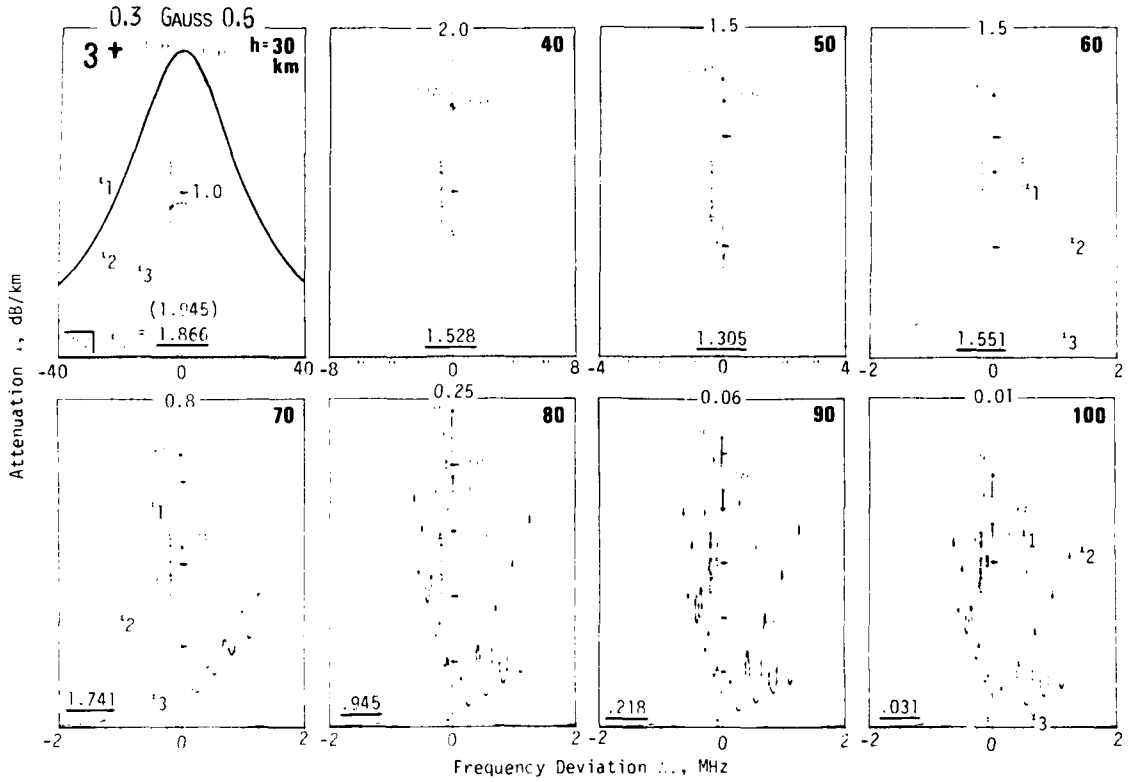

Fig. 7. Zeeman attenuation patterns of the oxygen microwave line $K = 3^+$ for altitudes h = 30–100 km (see Table 3). Each frame displays $\pi(\alpha_1)$, $\sigma^+(\alpha_2)$, and $\sigma^-(\alpha_3)$ patterns for the magnetic field strengths H = 0.3 (left hand) and H = 0.6 G (right hand). The patterns are symmetric with respect to the center axis (interchange σ^+ and σ^-). The frequency deviation $\Delta\nu = f - \nu_0$ is between ±40 MHz for h = 30 and ±2 MHz for h = 60–100 km. The maximum attenuation rate α_0 is that of the isolated unsplit line (H = 0); the value in parentheses is calculated with program P1. The values of $\alpha_1(\nu_0)$ in decibels per kilometer are for 0.3 (see Figure 9) and 0.6 G.

In principle, three different Zeeman patterns $\alpha_{1,2,3}$ are possible for any K^+ line. These patterns are obtained by evaluating all of the η and ξ coefficients in the π and $\sigma^\pm$ groups and applying a line shape such as (25). Each sum of sublines determines a Zeeman pattern according to

$$\alpha_{1,2,3} = \alpha_0 \sum_{M,K} \xi(M, K)/\{1 + [(f - \nu_0^z(M, K))/\gamma_h]^2\} \tag{28}$$

where

$$\alpha_0 = 0.182 f(a_1 p/\gamma_h)\vartheta^3 \exp[a_2(1 - \vartheta)] \quad \text{dB/km}$$

The unsplit line $H = 0$ follows from (28) by assuming $\xi(M, K) = 1$ and $\nu_0^z = \nu_0$. For more accurate calculations, the Lorentzian (equation (15)) in (28) may be replaced by the Voigt profile (Figure 5).

Additional information has to be provided before the mesospheric O_2 line pattern α_z can be calculated, that is, the polarization of the radio wave and its orientation with respect to the geomagnetic field **H**. For linearly polarized radiation an angle of orientation θ is defined between the wave's magnetic field component in a plane of constant phase (i.e., perpendicular to the direction of propagation) and the geomagnetic field direction **H**; for circularly polarized radiation the angle θ is defined between the plane of constant phase and **H**. A mesospheric O_2 line α_z then generally consists of a mixture of the three Zeeman patterns:

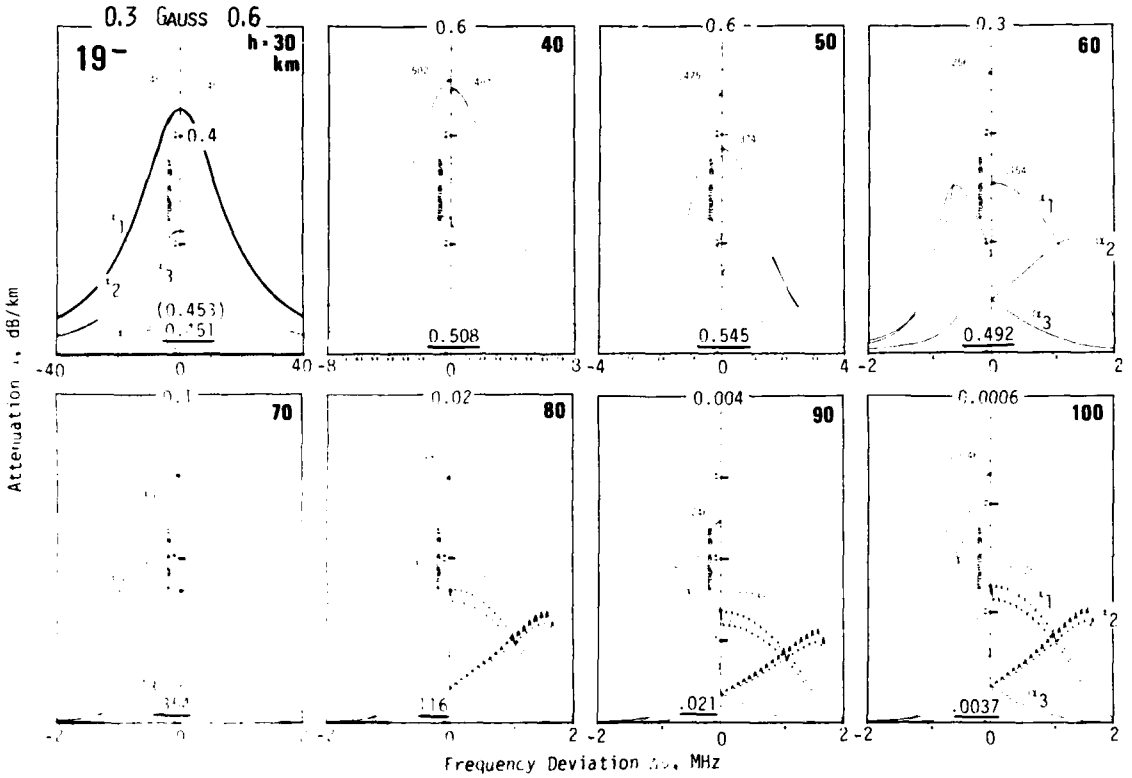

Fig 8. Same as Figure 7, except $K = 19$ oxygen microwave line.

Wave polarization	Zeeman pattern α_z
linear	$\alpha_1 \cos^2\theta + (\alpha_2 + \alpha_3)\sin^2\theta$
circular, right-handed	$2\alpha_2 \sin^2\theta + 0.5(\alpha_1 + \alpha_2 + \alpha_3)\cos^2\theta$
circular, left-handed	$2\alpha_3 \sin^2\theta + 0.5(\alpha_1 + \alpha_2 + \alpha_3)\cos^2\theta$

(29)

Equations (29) imply that mesospheric O_2 line attenuation is polarization and direction (anisotropic medium) dependent. Further coordinate transformation is necessary when a fixed antenna receives radiation from a mesospheric space element.

The patterns $\alpha_{1,2,3}$ of the O_2 lines $K = 1^{\pm}$ to $29^{\pm}$ have been calculated for local *p-T-H* conditions over the height range 30–100 km at two magnetic field strengths, $H = 0.3$ and 0.6 G. Two examples, $K = 3^{+}$ and 19 , are depicted in Figures 7 and 8. (The complete set $K^{\pm} = 1$–29 is available upon request (to be published in a report).) Above $h = 70$ km the individual, now mostly Doppler-broadened components become discernable. Although the details depend on specific K values, the overall features at given heights are similar to the cases illustrated in Figures 7 and 8 except for different scale factors.

The maximum of the pattern $\alpha_1(\nu_0)$ for $h = 30$–100 km is shown in Figure 9 covering $K = 1^{\pm}$ to $29^{\pm}$, so far as a threshold of 0.02 dB/km is exceeded. The $K^{\pm} = 19$ line pair has α values independent of height (temperature) over the range $h \approx 20$–50 km. The results, in combination with a beginning dissociation to atomic oxygen (e.g., at $h = 120$ km, $O_2/O = 0.25$), establish $h = 100$ km as the plausible boundary to outer space for radio path modeling. The cutoff height for water vapor is much lower ($h \approx 20$ km).

Having a full Zeeman picture at hand, one might

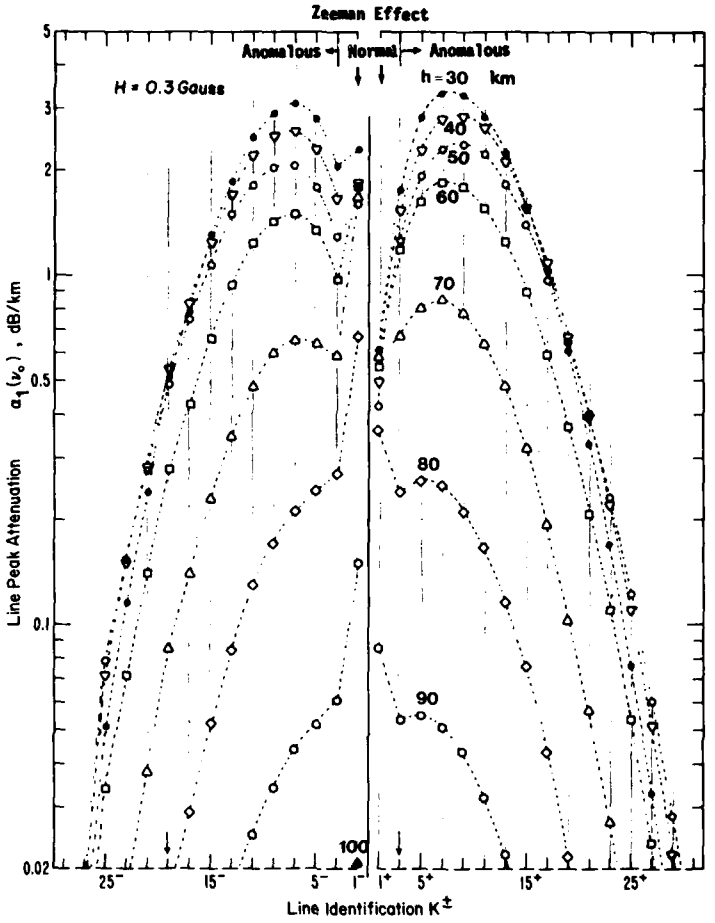

Fig. 9. Maximum attenuation $\alpha_1(\nu_0, H = 0.3\ \text{G})$ for the oxygen microwave lines, $K = 1^{+}$ to 29^{+} (Table 4*a*) at altitudes $h = 30$–100 km (see Table 3).

consider applications for this information. The uniform mixing of O_2 affords opportunities to remotely sense mesospheric temperature profiles $T(h)$ or geomagnetic field strength including variations, $H \pm dH$, via emmissions originating from $\alpha_z(h)$. A multiplet pattern is expanded, with increasing H, like an accordion (see Figure 7), at the most to $\nu_0 \pm 2.5$ MHz (equation (26)). Variations in the geomagnetic field strength H translate into height dependent changes of selective attenuation $\alpha_z(h)$. The example in Figure 10 reveals that the response $\delta(dH)$ for $\alpha_1(\nu_0)$ is most pronounced in the region $h = 60$–70 km.

Power saturation of a mesospheric O_2 Zeeman pattern is our final concern. An active system (i.e., radar), in principle, can diminish or even eliminate the calculated attenuation α_z. A rough estimate for the onset of saturation effects yields that the radiated power density at ν_0 needs to exceed values on the order of $0.5p^2$ in units of W cm^{-2} Pa^{-2}, which is not out of the question above $h = 70$ km.

5. CONCLUSION

Moist air was characterized as an atmospheric propagation medium. The basic physics of molecular absorption in a radio path have been cast into a model with optimum computer run time, but

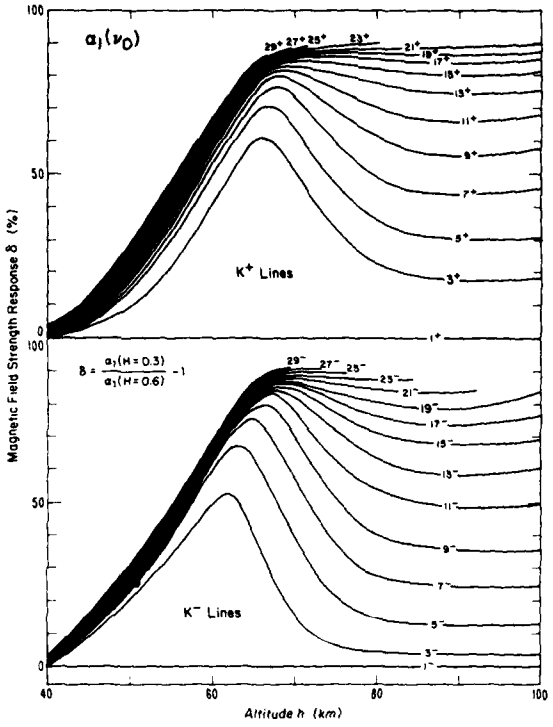

Fig. 10. Response δ of the maximum attenuation $\alpha_1(\nu_0)$ in percent to an equal percentage drop in the magnetic field strength H over the altitude range h = 40–100 km (see Table 3) for the oxygen microwave lines $K = 1^{\pm}$ to $29^{\pm}$.

without undue approximations. The paper has expanded upon an EHF version (30–300 GHz) by *Liebe and Gimmestad* [1978] in terms of frequency and height coverages and has provided graphical and numerical examples. In addition, the formulation of dispersion has been clarified. Shortcomings of the present model lie in the omitted spectroscopic data base for trace gases, and in the lack of a model that describes the *RH*-dependent water uptake (i.e., w) by various atmospheric aerosol distributions [*Nilsson*, 1979].

Use of programs P1 and P2 is straightforward. The routines (available in FORTRAN IV upon request) are operated, even by nonexpert users, simply by calling the program name, choosing from a battery of model atmospheres, and typing in the interactively requested input parameters within the limits of (9): meteorological data are converted into propagation data. Detrimental effects such as fluctuations in amplitude, phase, and group velocities, and the direction of the radio wave may be predicted from spatial and temporal variations of *P-RH-T*. A priori assessments can be made of rare events for reliable system operations and of possible bandwidth limitations.

The model may serve as a reference for comparison with current research. This is especially valuable with respect to studies of water vapor excess absorption, which is accounted for only by an empirical correction. A reliable expression for refractivity $N(f, P, RH, T, H, \theta)$ would be a boon to workers in the field since N (equation (2)) is at the hub of all millimeter and submillimeter propagation problems through the nonprecipitating atmosphere. An important task ahead is research into the nature of H_2O excess absorption, already underway in several laboratories including ours at the Institute for Telecommunication Sciences, NTIA.

Acknowledgments. The author wishes to thank B. Shaw for his skillful computer programing. The work was supported by the U.S. Army Research Office under contract ARO 42-80.

REFERENCES

Birnbaum, G. (1953), Millimeter wavelength dispersion of water vapor, *J. Chem. Phys.*, *21*(1), 57–61.

Bögel, W. (1977), Neue Näherungsgleichungen für den Sättigungsdruck des Wasserdampfes, *DFVLR Ber. DLR-FB 77-52*, Wissenschaftliches Berichtswesen, Deutsche Forschungs- und Versuchsanstalt für Luft- und Raumfahrt, Cologne, West Germany.

Carlon, H. R., and C. S. Harden (1980), Mass spectrometry of ion-induced water clusters: An explanation of the infrared continuum absorption, *Appl. Opt.*, *19*(11), 1776–1786: (Addenda, *Appl. Opt.*, *20*(5), 726–727.

Chang, A. T., and T. T. Wilheit (1979), Remote sensing of atmospheric water vapor, liquid water, and wind speed at the ocean surface by passive microwave techniques from the NIMBUS 5 satellite, *Radio Sci.*, *14*(5), 793–802.

Crane, R. (1980), Attenuation estimates for millimeter wave windows near 94, 140 and 220 GHz, *ERT Doc. P-A502*, Environ. Res. & Technol., Inc., Concord, Mass., May.

Crane, R. (1981), Fundamental limitations caused by RF propagation, *Proc. IEEE*, *69*(2), 196–209.

Ellsaesser, H. W., J. E. Harries, D. Kley, and R. Penndorf (1980), Stratospheric H_2O, *Planet. Space Sci.*, *28*, 827–835.

Emery, R. J., A. M. Zavody, and H. A. Gebbie (1980), Measurements of atmospheric absorption in the range 5–17 cm^{-1} and its temperature dependence, *J. Atmos. Terr. Phys.*, *42*, 801–807.

Faddeyea, V. N., and N. M. Tarentev (1961), *Tables of the Probability Integral for Complex Argument*, Pergamon, New York.

Falcone, V. J., Jr., L. W. Abreu, and E. P. Shettle (1979), Atmospheric attenuation of millimeter and submillimeter waves: Models and computer code, *Environ. Res. Paper 679*, October (available as *Rep. AFGL-TR-79-0253*, U.S. Air Force Geophys. Lab., Hanscom Air Force Base, Mass.).

Harries, J. E. (1980), Atmospheric radiometry at submillimeter wavelengths, *Appl. Opt.*, *19*(18), 3075–3081.

Hill, R. J., and S. F. Clifford (1981), Contributions of water vapor monomer resonances to fluctuations of refraction and absorption for submillimeter through centimeter wavelengths, *Radio Sci.*, *16*(1), 77–82.

Hill, R. J., S. F. Clifford, and R. S. Lawrence (1980), Refractive index and absorption fluctuations in the infrared caused by temperature, humidity, and pressure fluctuations, *J. Opt. Soc. Am.*, *70*(10), 1192–1205.

Hopponen, J. D. (1980), Simulation of EHF propagation through the atmosphere, *AGARD Conf. Proc., AGARD-CP-284*, 6/1–6/11.

Kemp, A. J., J. R. Birch, and M. N. Afsar (1978), The refractive index of water vapor: A comparison of measurement and theory, *Infrared Phys.*, *18*, 827–833.

Lam, K. S. (1977), Application of pressure-broadening theory to the calculation of atmospheric oxygen and water vapor microwave absorption, *J. Quant. Spectros. Radiat. Transfer*, *17*, 351–383.

Lenoir, W. B. (1968), Microwave spectrum of molecular oxygen in the mesosphere, *J. Geophys. Res.*, *73*(1), 361–376.

Liebe, H. J. (1980), Atmospheric water vapor: A nemesis for millimeter wave propagation, in *Atmospheric Water Vapor*, edited by A. Deepak, T. Wilkerson, and L. Ruhnke, pp. 143–201, Academic, New York.

Liebe, H. J., and G. G. Gimmestad (1978), Calculation of clear air EHF refractivity, *Radio Sci.*, *13*(2), 245–251.

Liebe, H. J., G. G. Gimmestad, and J. D. Hopponen (1977), Atmospheric oxygen microwave spectrum—Experiment versus theory, *IEEE Trans. Antennas Propag.*, *AP-25*(3), 327–335.

Nilsson, B. (1979), Meteorological influence on aerosol extinction in the 0.2–40-μm wavelength range, *Appl. Opt.*, *18*(20), 3457–3473.

Pierluissi, J. H., P. C. Vanderwood, and R. B. Gomez (1977), Fast algorithm for the Voigt profile, *J. Quant. Spectros. Radiat. Transfer*, *18*, 555–558.

Poynter, R. L., and H. M. Pickett (1980), Submillimeter, millimeter, and microwave spectral line catalogue, *JPL Publ. 80-23*, Jet Propul. Lab., NASA, Pasadena, Calif., June.

Rosenkranz, P. W. (1975), Shape of the 5 mm oxygen band in the atmosphere, *IEEE Trans. Antennas Propag.*, *AP-23*(4), 498–506.

Rothman, L. S. (1981), AFGL atmospheric absorption line parameters compilation: 1980 version, *Appl. Opt.*, *20*(5), 791–795.

Rothman, L. S., et al. (1981), AFGL trace gas compilation: 1980 version, *Appl. Opt.*, *20*(8), 1323–1328.

Simpson, O. A., B. L. Bean, and S. Perkowitz (1979), Far infrared optical constants of liquid water measured with an optically pumped laser, *J. Opt. Soc. Am. Lett.*, *69*(12), 1723–1726.

Smith, E. W. (1981), Absorption and dispersion in the O_2 microwave spectrum at atmospheric pressures, *J. Chem. Phys.*, *74*(12), 6658–6673.

Smith, E. W., and M. Guiraud (1979), Pressure broadening of the O_2 microwave spectrum, *J. Chem. Phys.*, *71*(11), 4209–4217. (Errata, *J. Chem. Phys.*, *74*(1), 335.)

Stankevich, K. S. (1974), Absorption of submillimeter-range radio waves in a dry atmosphere, *Izv. Vyssh. Uchebn. Zaved. Radiofiz.*, *17*(5), 764–766. (*Radiophys. Quantum Electron.*, Engl. Transl., *17*, 579–581, 1974.)

Van Vleck, J. H. (1947), The absorption of microwaves by oxygen and uncondensed water vapor, *Phys. Rev.*, *71*(7), 413–433.

Waters, J. R. (1976), Absorption and emission by atmospheric gases, in *Methods of Experimental Physics*, vol. 12B, edited by M. L. Meeks, chap. 2.3., Academic, New York.

Unclassified
SECURITY CLASSIFICATION OF THIS PAGE (When Data Entered)

REPORT DOCUMENTATION PAGE		READ INSTRUCTIONS BEFORE COMPLETING FORM
1. REPORT NUMBER 16638.7-GS	2. GOVT ACCESSION NO. AD-A112 928 N/A	3. RECIPIENT'S CATALOG NUMBER N/A
4. TITLE (and Subtitle) Modeling Attenuation and Phase of Radio Waves in Air at Frequencies Below 1000 GHz		5. TYPE OF REPORT & PERIOD COVERED Reprint 6. PERFORMING ORG. REPORT NUMBER N/A
7. AUTHOR(s) Hans J. Liebe		8. CONTRACT OR GRANT NUMBER(s) ARO MIPR 6-82
9. PERFORMING ORGANIZATION NAME AND ADDRESS Institute for Telecommunication Sciences Boulder, CO 80303		10. PROGRAM ELEMENT, PROJECT, TASK AREA & WORK UNIT NUMBERS N/A
11. CONTROLLING OFFICE NAME AND ADDRESS U. S. Army Research Office P. O. Box 12211 Research Triangle Park, NC 27709		12. REPORT DATE Nov-Dec 81 13. NUMBER OF PAGES 17
14. MONITORING AGENCY NAME & ADDRESS(if different from Controlling Office)		15. SECURITY CLASS. (of this report) Unclassified 15a. DECLASSIFICATION/DOWNGRADING SCHEDULE
16. DISTRIBUTION STATEMENT (of this Report) Submitted for announcement only.		
17. DISTRIBUTION STATEMENT (of the abstract entered in Block 20, if different from Report)		
18. SUPPLEMENTARY NOTES		
19. KEY WORDS (Continue on reverse side if necessary and identify by block number)		
20. ABSTRACT (Continue on reverse side if necessary and identify by block number)		

DD FORM 1 JAN 73 1473 EDITION OF 1 NOV 65 IS OBSOLETE

Unclassified
SECURITY CLASSIFICATION OF THIS PAGE (When Data Entered)